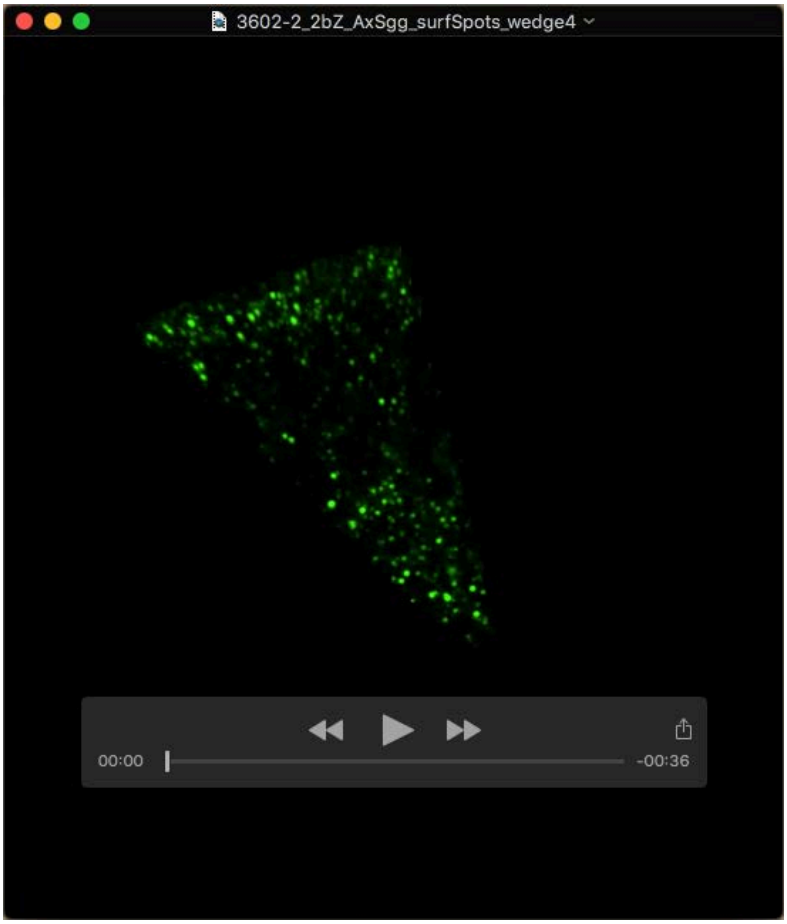

Movie 1

Axin^{M}-Sgg BiFC in the domain of low Wg of signaling detected using super-resolution microscopy (Airyscan).

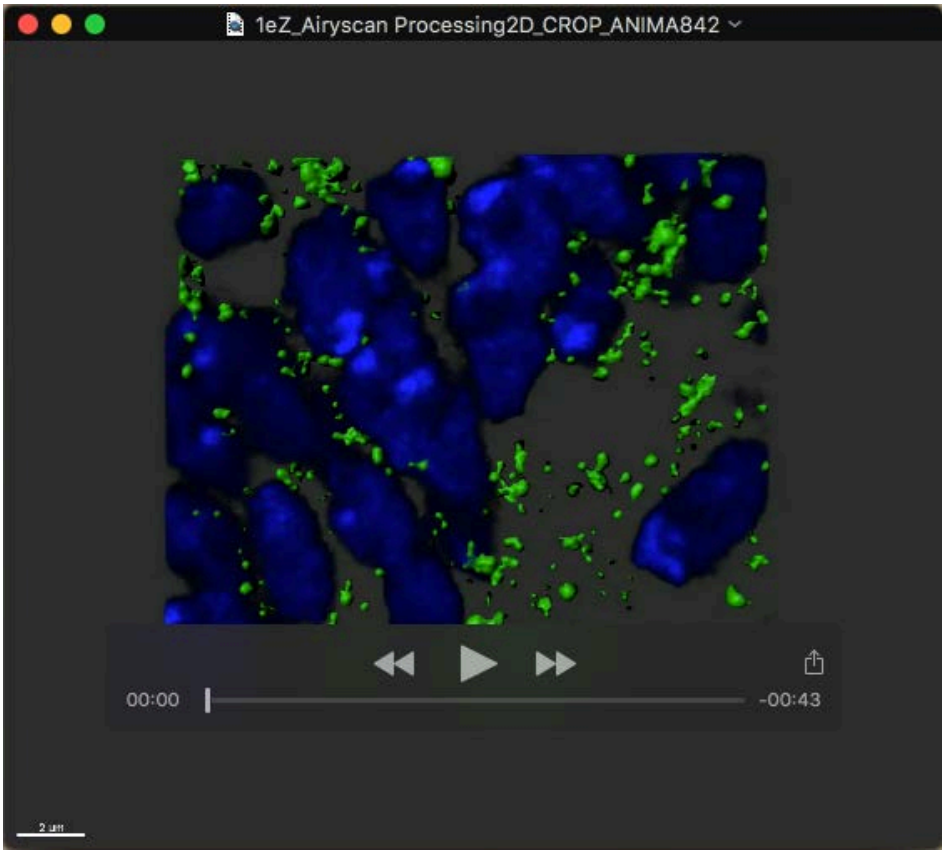

Movie 2

In the domain of low Wg signaling, nuclei (blue) are surrounded by Axin^{M}-Sgg objects BiFC (green) visualized using Imaris® (see also Fig. 2A).

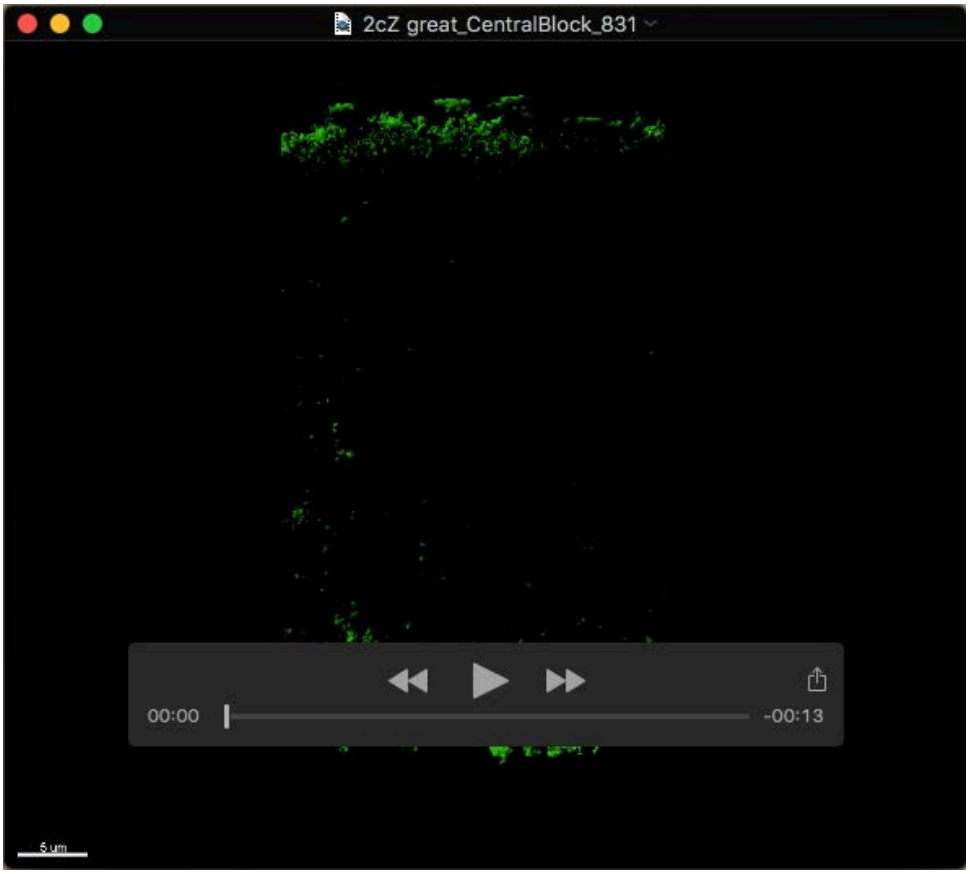

Movie 3

In the domain of strongest Wg signaling, Axin^{M}-Sgg BiFC objects (green) are depleted around nuclei (blue).

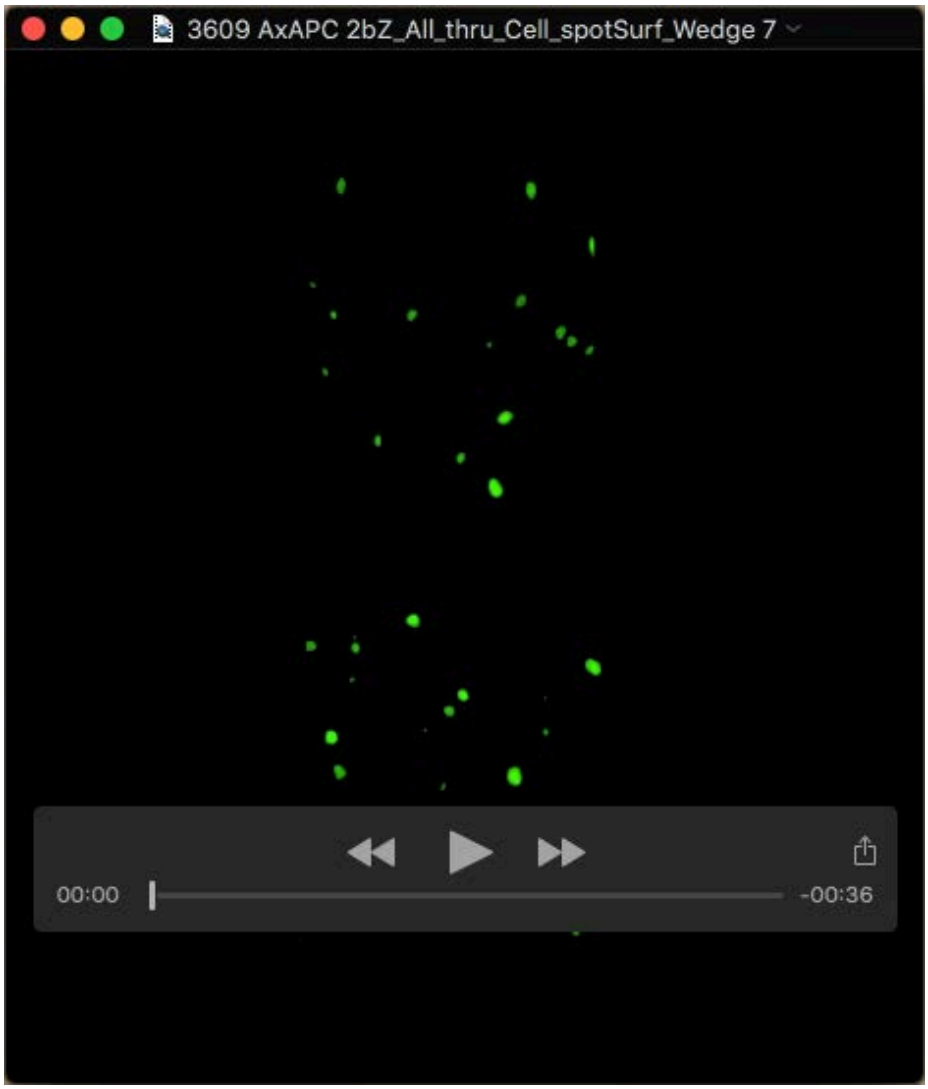

Movie 4

In the domain of strongest Wg signaling, ^{N}Axin-APC2 BiFC (green) super-complexes co-localizing with α-catenin (red) are shown using surface view in Imaris ® (see also Fig. 4A).

Supplementary Data (Lybrand et al.)

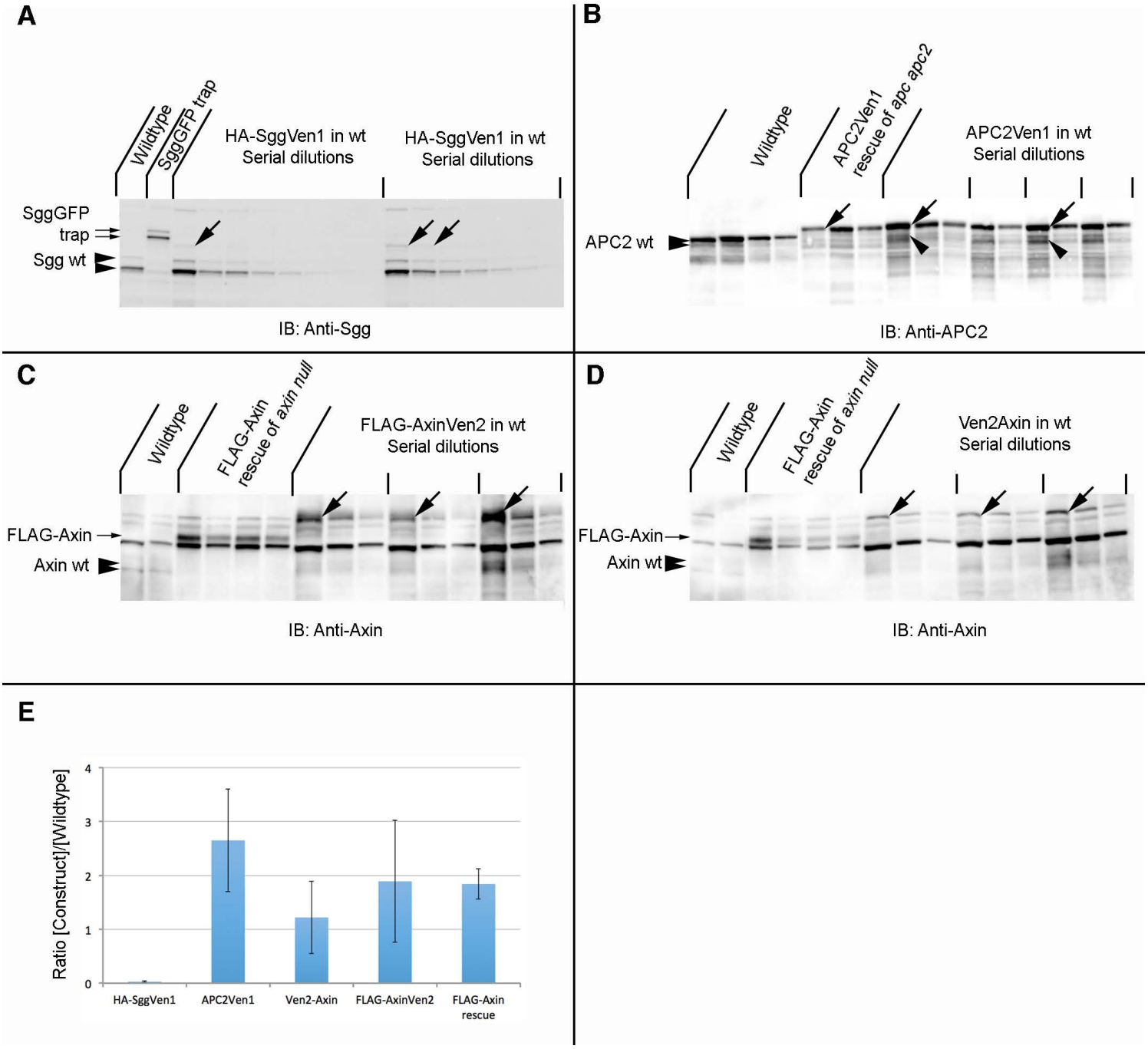

Figure S1 The tubulin promoter drives fusion protein expression near the physiological range of wild type proteins. (A) Immunoblot with monoclonal antibody 4G-E1 reveals two Sgg isoforms (54 kDa and 59 kDa; arrowheads) in wild type *Drosophila* larval lysate. Confirming these bands as Sgg isoforms, an intron insertion of GFP in the Sgg locus expresses Sgg-GFP fusion proteins: wild type bands (54 kDa, 59k kDa) are shifted to lower mobility (81 kDa, 86 kDa) than native Sgg proteins. Immunoblot of serial 2-fold dilutions of lysate from larvae expressing a HA-SggVen1 construct indicates presence of a band with lower mobility (77 kDa) than wild type Sgg. Expression of four independent sample preparations was quantified from 12 lanes of two different blots. (B) Detection of APC2 proteins by guinea pig anti-APC2 serum (Takacs et al.) reveals wild type APC2 in control larval extracts (114, 117 kD, arrowheads), which are absent in *apc apc2* null animals rescued by tubulin promoter-driven expression of APC2Ven1 (predicted MW 135 kD, arrows). Wild type APC2 proteins and APC2Ven1 are detected in wild type animals expression APC2Ven1. Expression of four independent samples from 15 lanes of two blots was quantified. (C,D) Detection of Axin by guinea pig anti-Axin polyclonal serum (Wang et al.) reveals wild type Axin (77, 82 kD), which is absent in *axin* null larvae rescued by tubulin promoter-driven expression of FLAG-Axin (Peterson-Nedry et al.). Background bands are present and co-migrate with extracts from wild type animals expressing FLAG-AxinVen2 (predicted MW 100.1 kD) in (C) and wild type animals expressing Ven2Axin (predicted MW 92kD) in (D). The relative intensity of background bands in wild type extracts was used to subtract background signal in the bands of Axin constructs. Similarly, we determined levels of FLAG-Axin in rescue animals relative to wild type (shown in (E)). Four independent extracts were prepared for each of the two constructs, quantified from 12 lanes each from two blots. (E) AzureSpot® software was used to determine levels of band intensity (Materials and Methods). The ratio of expressed construct to endogenous protein was calculated in Excel. Mean values and standard deviation are shown.

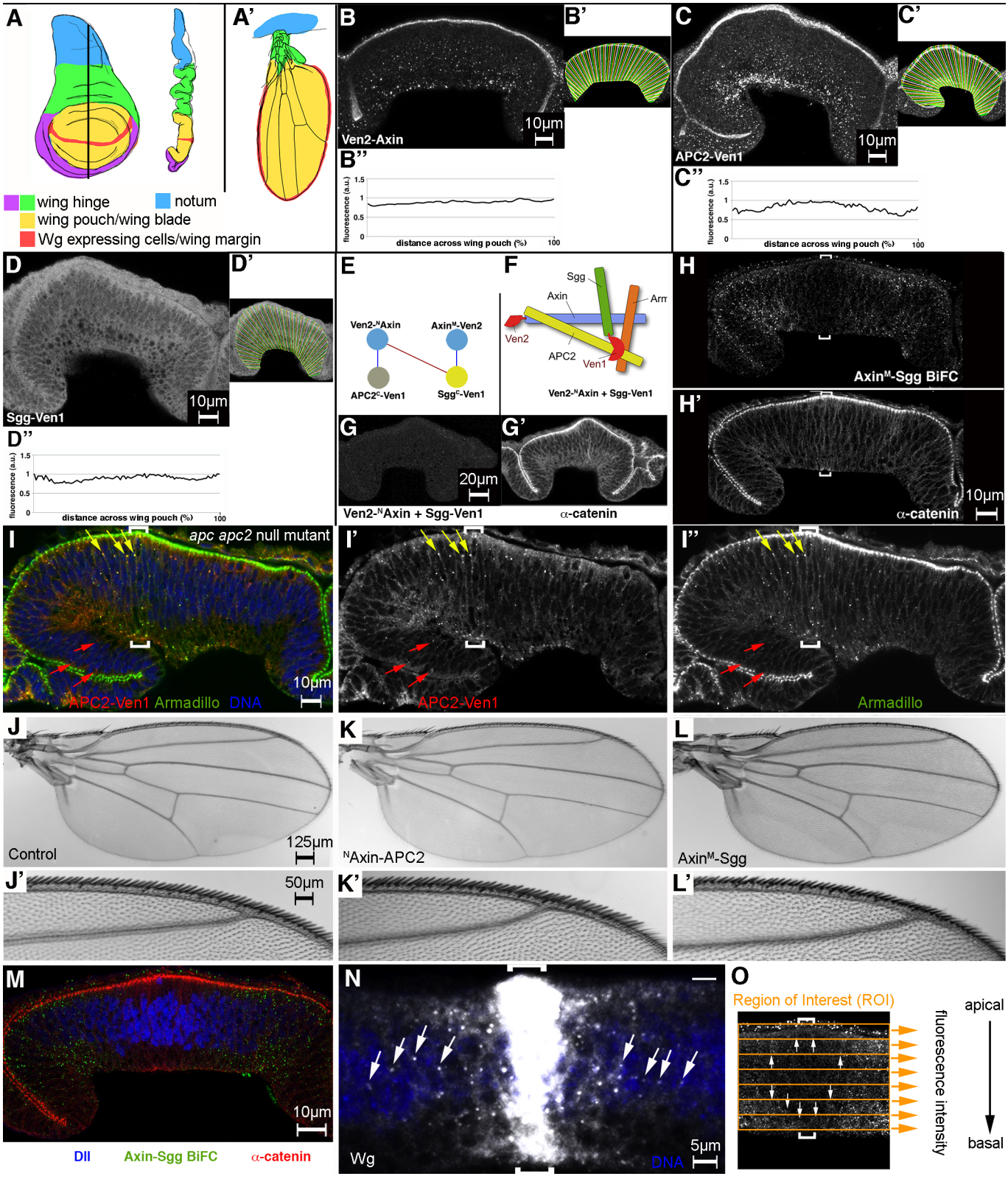
A
A'
wing hinge
notum
wing pouch/wing blade
Wg expressing cells/wing margin
B
B'
B''
Ven2-Axin
10μm
fluorescence (a.u.)
distance across wing pouch (%)
C
C'
C''
APC2-Ven1
D
D'
D''
Sgg-Ven1
E
Ven2-NAxin
AxinM-Ven2
APC2C-Ven1
SggC-Ven1
F
Sgg
Axin
Arm
Ven2
APC2
Ven1
Ven2-NAxin + Sgg-Ven1
G
G'
20μm
Ven2-NAxin + Sgg-Ven1
α-catenin
H
AxinM-Sgg BiFC
H'
α-catenin
I
apc apc2 null mutant
APC2-Ven1 Armadillo DNA
I'
APC2-Ven1
I''
Armadillo
J
Control
125μm
K
NAxin-APC2
L
AxinM-Sgg
J'
50μm
K'
L'
M
Dll
Axin-Sgg BiFC
α-catenin
N
Wg
DNA
5μm
O
Region of Interest (ROI)
fluorescence intensity
apical
basal

Figure S2

Axin, APC2 and Sgg protein levels are not modulated by the Wg gradient but BiFC is regulated. **(A)** Wing imaginal disc in 'top-down' and side-view (equivalent to view in cryosections). The color-coding in the fate map illustrates the band of Wg expressing cells bisecting the wing pouch (red, A) forms the wing margin in the adult wing **(A')**. The wing pouch (yellow) folds about the Wg stripe to generate the upper and lower wing blade (only the upper blade is visible in A'). Green domain forms the wing hinge, blue colored tissue part of the thorax (modified from Zimmerman et al., 2010). (B-D) Cryosections of wing discs are shown and the quantification of expressed components illustrated (Materials and Methods).

(B) Expression of Ven2-Axin was detected with anti-GFP antibody; quantification in ImageJ reveals even protein distribution (B',B"). APC2-Ven1 was also detected by anti-GFP immunostaining; quantification in **(C',C")** shows even protein levels. **(D)** Sgg-Ven1, detected by the HA epitope, shows ubiquitous and even protein expression (D', D"; this is the disc shown in Fig. 1E). **(E, F)** The specificity of the BiFC method is illustrated by patterned BiFC of (Ven2-^{N}Axin + APC2-Ven1) and (Axin^{M}-Ven2 + Sgg-Ven1)(blue lines; see text) and lack of specific BiFC by the pair (Ven2-^{N}Axin + Sgg-Ven1) (red line). **(G)** The combination (Ven2-^{N}Axin + Sgg-Ven1) does not yield specific BiFC signal; the image is artificially enhanced to reveal background. This disc is counterstained for α-catenin **(G')**. **(H)** Monochrome images of Fig. 1H are shown. **(I, I', I")** tubulin-promoter driven expression of Ven1 tagged APC2 rescues the *apc apc2* null mutant. A cryosection stained with an APC2-specific antibody (McCartney et al., 1999) and counterstained for Armadillo, reveals co-localization in prominent foci (yellow arrows; PCC = 0.58; MCC[Arm] = 0.10; MCC[APC2] = 0.02) near Wg-expressing cells, indicated by brackets). Similar foci of APC2 in cells exposed to little Wg, show a lesser degree of co-localization with Armadillo (red

arrows; PCC = 0.29; MCC[Arm] = 0.48; MCC[APC2] = 0.28). These two populations are consistent with the localization of inactive and active DCs, respectively (see text). The detected co-localization of APC2 and Armadillo in lateral regions results from uniform small size foci and variable size and intensity APC2 foci, possibly reflecting another function (not shown). **(J-L)** Expression of tubulin-promoter driven expression of ^{N}Axin-APC2 and Axin^{M}-Sgg BiFC constructs does not interfere with wing development. **(J, J')** Control wing of *y w* female and magnified view of the anterior margin, which serves as a sensitive indicator for changed in Wg signaling (J'). **(K, K')** Wing of female fly constitutively expressing ^{N}Axin-APC2 BiFC constructs; both are rescue constructs and no defects are observed. **(L, L')** Wing of female fly shows no defects after ubiquitous expression of Axin^{M}-Sgg BiFC constructs throughout the 3rd larval instar (see text). **(M)** Dll protein stain (blue) of the wing disc shown in Fig. 1H,I, S1H. **(N)** Wg stain (white) reveals Wg foci predominantly in the nuclear zone (arrows, nuclei in blue). Note that only a small fraction of Wg is detected outside Wg-expressing cells, indicating tight control of endocytosis. An overexposed 5 µm Z-projection is shown. **(O)** Schematic illustrating quantification in Fig. 1M. Fluorescence intensity in 80 rectangular regions of interest (ROI, orange rectangles, shown for 8 ROI) was quantified along the apical-basal axis, averaged for 7 image stacks, then intensity was plotted against the relative apicobasal position.

Scale bars are 10 µm in (B-D,H-I,M), 20 µm in (G) 125 µm in (J,K,L), 50 µm in (J',K',L'), 5 µm in (N).

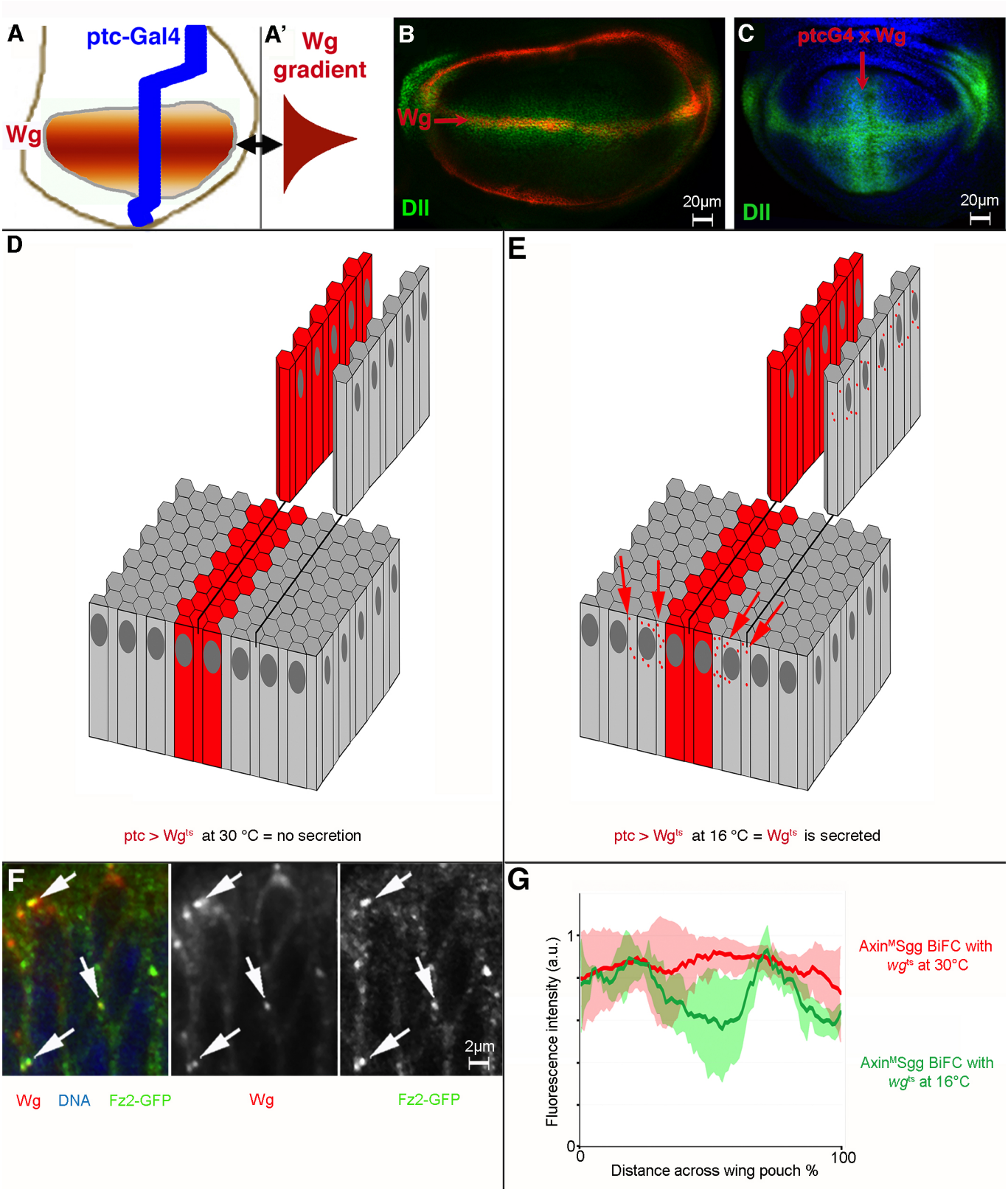

Figure S3

Ectopic Wg expression induced orthogonal to the endogenous Wg gradient in developing wing discs. (A, A') Schematic representation of the endogenous Wg gradient (red; double-headed arrow). *ptc*>Gal4 is expressed in an band (blue) orthogonal to Wg. **(A')** Schematic of the Wg gradient (red). **(B)** Endogenous Wg expression (red) induces the Wg target gene Dll (green). **(C)** Ectopic Wg expression (not shown) under the control of *ptc*>Gal4 induces ectopic Dll expression (Dll, green). **(D, E)** Schematic of *ptc*-driven expression of Wg^{ts} (red) and a row of distant cells (gray). **(D)** At non-permissive temperature (30°C), Wg^{ts} cannot be secreted and is confined to expressing cells (red), contrasting with Wg^{ts} secretion that occurs at permissive temperature (16°C) **(E)**, when expressing cells signal to distant cells (gray) and to each other (arrows). **(F)** Wg foci co-localize with Fz2-GFP foci 30 minutes after induction (arrows; PCC = 0.6058 MCC = 0.6135, 0.3778), indicating Wg foci as sites of ligand-activated receptor. **(G)** $Axin^{M}$Sgg BiFC fluorescence intensity profiles (arbitrary units) across the wing pouch of animals without inactivation of wg^{ts} (green line) or with inactivation of wg^{ts} (red line). Shaded areas represent variation within one standard deviation.

Scale bar 20μm in (B,C), 2 μm in (F).

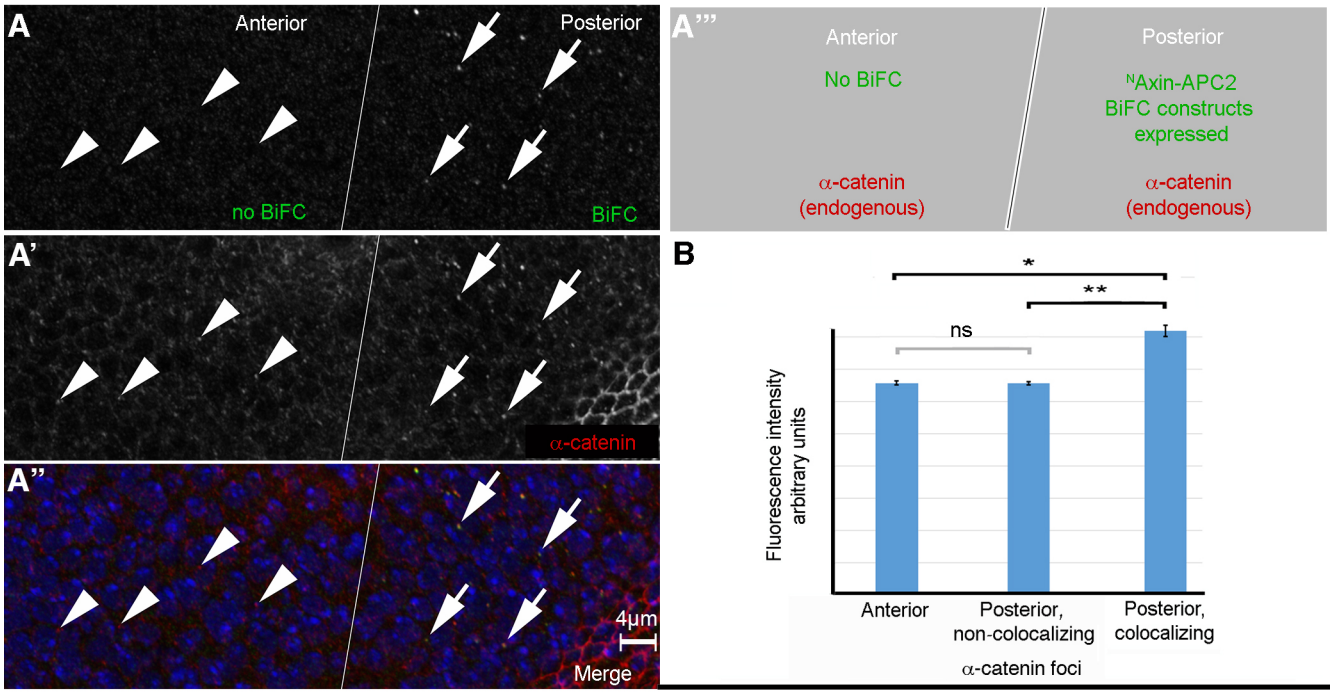

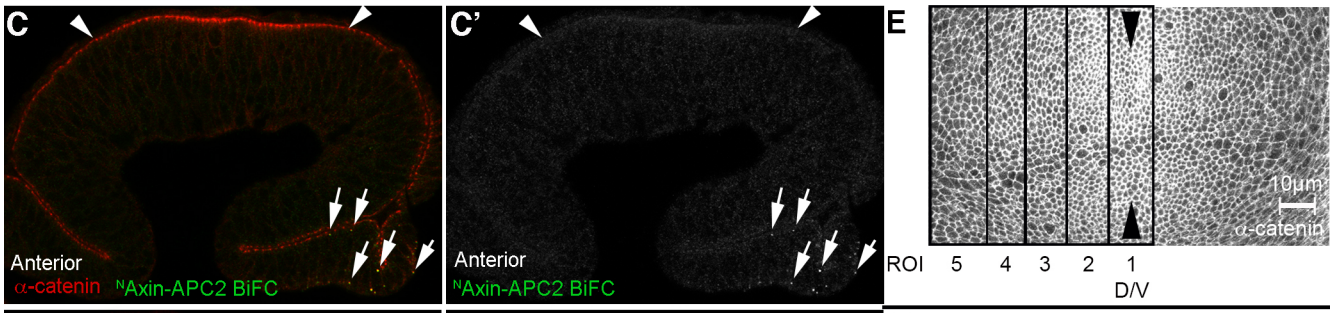

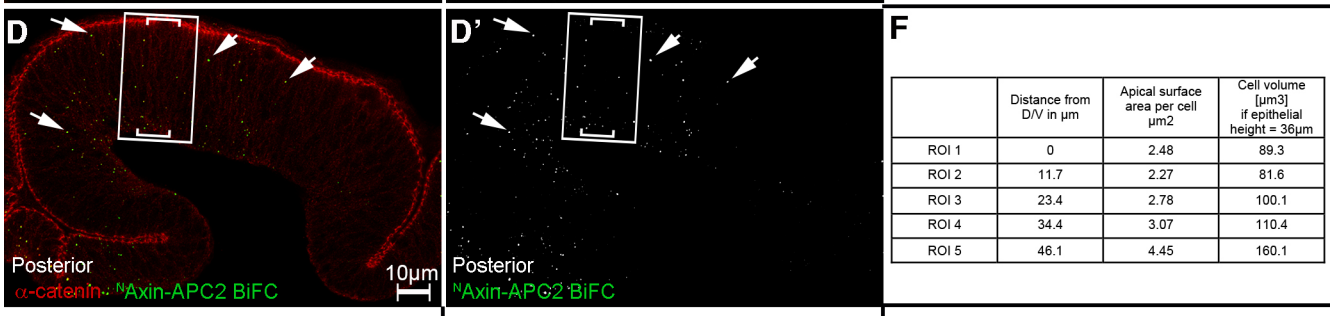

F

	Distance from D/V in μm	Apical surface area per cell μm2	Cell volume [μm3] if epithelial height = 36μm
ROI 1	0	2.48	89.3
ROI 2	11.7	2.27	81.6
ROI 3	23.4	2.78	100.1
ROI 4	34.4	3.07	110.4
ROI 5	46.1	4.45	160.1

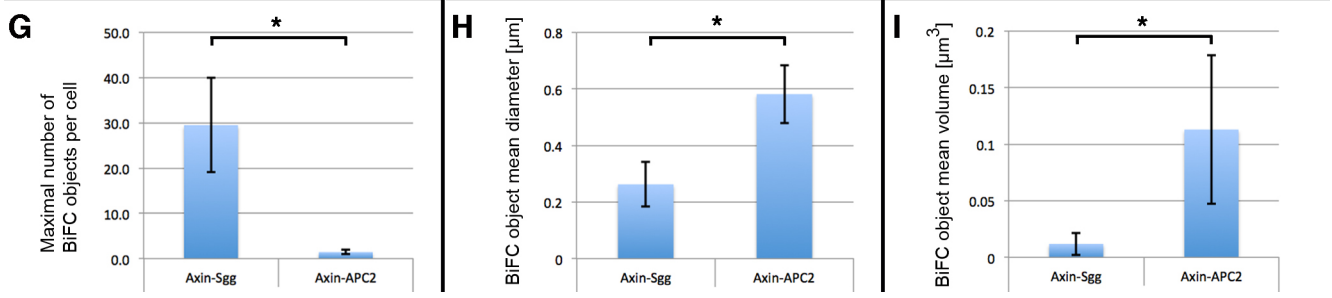

Figure S4

Expression of ^{N}Axin-APC2 moderately increases fluorescence intensity of α-catenin foci. (A) Expression of ^{N}Axin-APC2 BiFC constructs in only the posterior part of the wing disc (via Hh-Gal4 tub>Gal80^{ts} UAS>flipase; gray scale in A, green in merge in A") allows a comparison of α-catenin foci without (anterior) or with expression of ^{N}Axin-APC2 BiFC (posterior), which appear more intense in the posterior region (gray scale in A', red in merge in A"). The lattice on the right of the image is apical stain of α-catenin at adherens junctions. A schematic for the expression of α-catenin and ^{N}Axin-APC2 BiFC is shown in (A"'). **(B)** Foci of α-catenin modestly increase in fluorescence intensity if ^{N}Axin-APC2 BiFC is expressed. α-catenin foci that co-localize with ^{N}Axin-APC2 BiFC display significantly increased fluorescence intensity compared to anterior foci (*, $P<8.2x10^{-16}$) or non-colocalizing foci in the posterior compartment (**, $P<1.6x10^{-15}$) but not between non-colocalizing populations ($P\geq0.95$; ns, not significant)**. (C, D)** For quantification of ^{N}Axin-APC2 BiFC objects, construct expression was restricted to the posterior compartment (as for Fig. S4A-B; see Fig. S7 for schematic for these planes of sections); fluorescence levels in the anterior (non-expressing) compartment represent background (arrowheads, C,C'); the slanting section cuts through posterior tissue where true BiFC signal is evident (arrows). This allows background subtraction in a section through the posterior of the same disc (D), revealing distinct BiFC foci. Imaris® was used to calibrate background subtraction (Materials and Methods). The number of BiFC objects contained in a region flanking 10 μm either side of the D/V boundary (Wg expressing cells) was determined from a Z-stack in Imaris®. (E) Volume of a wing disc cell near the D/V boundary was determined as follows: all cells in a pseudostratified epithelium reach the apical surface which is outlined by α-catenin staining of adherens junctions. We determined the number of cells present in a region of interest (ROI) (E), which provides an average value for the apical surface of a cell

(F). This surface area (~2.48 μm^2) multiplied with the height of the epithelium (~36µm) provides an estimate for the average cell volume (89.3 μm^3). The apical surface area increases significantly as cells are ~46µm from the D/V boundary, as they adopt a wedge-like shape (Fig. 1H, and not shown) but all cells in the wing pouch are likely of similar volume. (G) An average of 1.45 (±0.48, s.d.) ^{N}Axin-APC2 BiFC objects are present per cell in the domain of maximal signaling (91 ^{N}Axin-APC2 BiFC objects in 66 cells from five sample volumes of interest). For Axin^{M}-Sgg BiFC, maximally 29.51 (±10.46, s.d.) were present per cell (1425 foci in 48 cells from four sample volumes). This difference in object number per cell by the two BiFC complexes is statistically significant (*, t-test, two-tail P<0.0005). (H) The apparent mean diameter is significantly different between objects of Axin^{M}-Sgg BiFC (0.26 µm ±0.08, s.d.; n=213) and ^{N}Axin-APC2 BiFC (0.58 µm ±0.10, s.d.; n=96; *, t-test, two-tail P< 3×10^{-93}). (I) Calculated apparent sphere volumes are significantly different between objects of Axin^{M}-Sgg BiFC (0.012 μm^3 ±0.010, s.d., n=213) and ^{N}Axin-APC2 BiFC (0.113 μm^3 ±0.066, s.d., n=96; *, t-test, two-tail P< 7×10^{-65}); the apparent volume is ~9.5x larger for ^{N}Axin-APC2 than for Axin^{M}-Sgg BiFC objects.

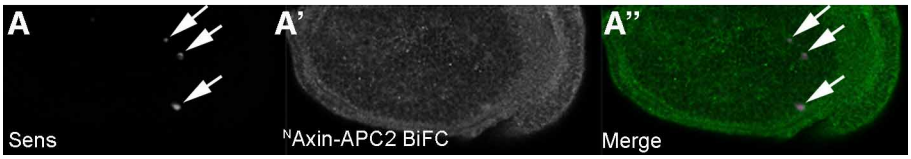

Figure S5

Prolonged inactivation of signaling (24 hours) abolishes both ^{N}Axin-APC2 BiFC and Senseless expression. (A) Remaining Sens expression in the lateral region of the disc (arrows) is known to be Wg-independent (Jafar-Nejad et al., 2006), serving as an internal control **(A')** no ^{N}Axin-APC2 BiFC is detectable above background levels (background was enhanced for context).

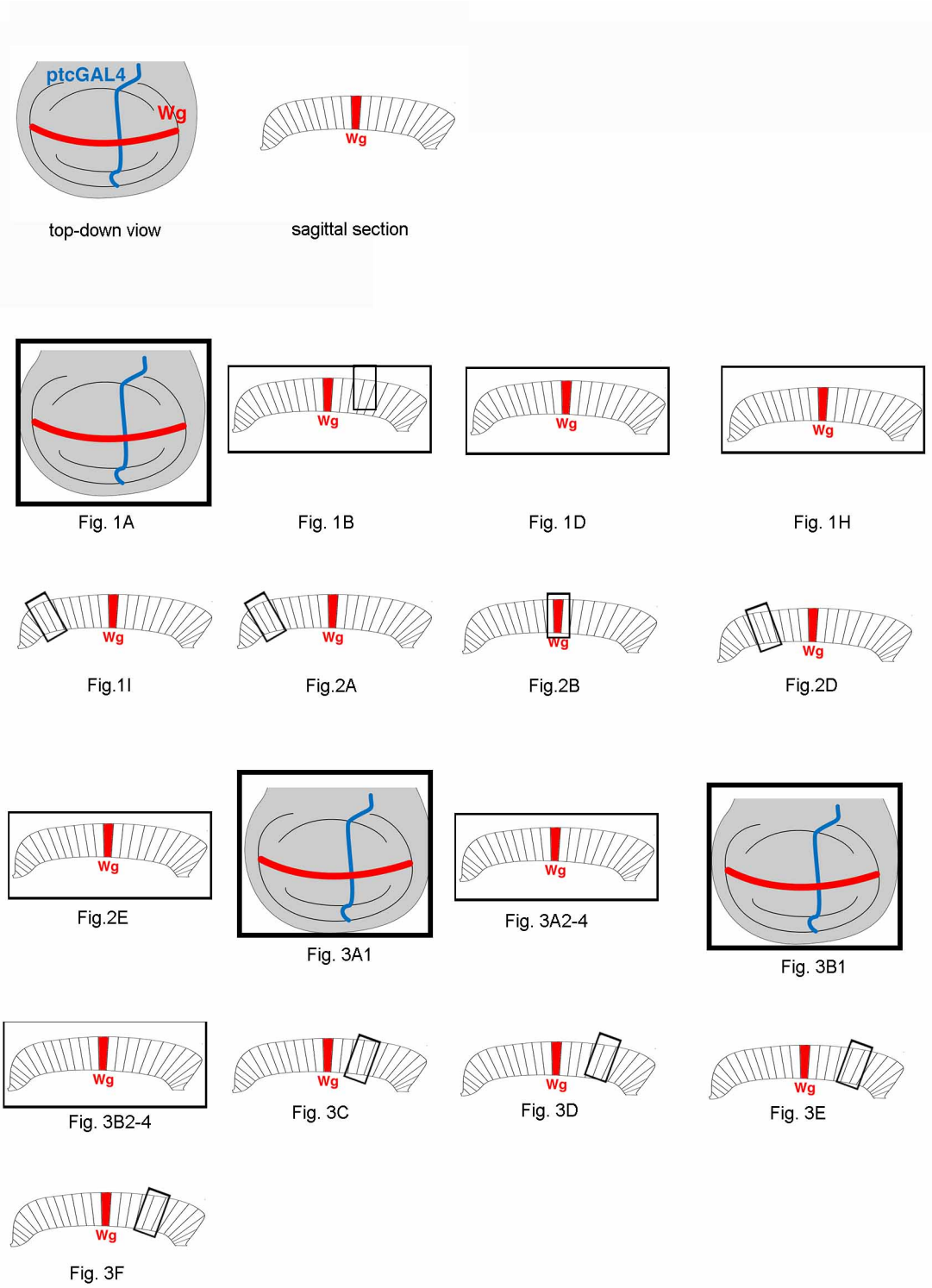

Figure S6. Location and orientation of images presented in Figs. 1-3. Schematic representation where images were taken in the wing disc.

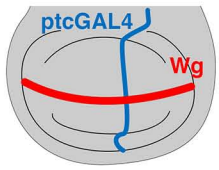

top-down view

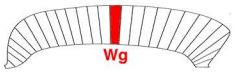

sagittal section

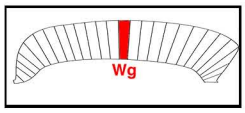

Fig. 4A

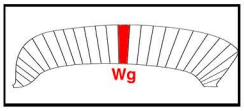

Fig. 4D

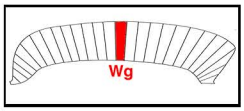

Fig. 4E

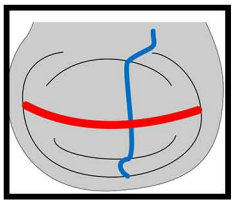

Fig. 4F

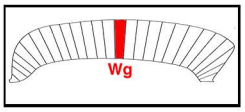

Fig. 5A

Fig. 5B

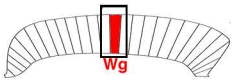

Fig. 5C

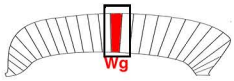

Fig. 5D

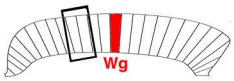

Fig. 5E

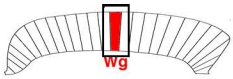

Fig. 5F

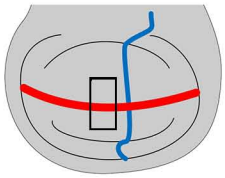

Fig. 5G

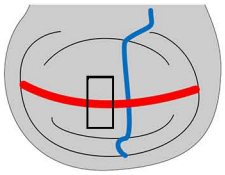

Fig. 5H

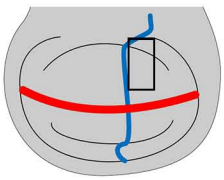

Fig. 6A

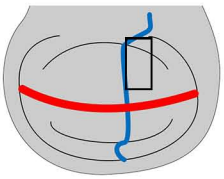

Fig. 6B

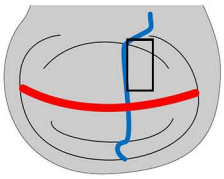

Fig. 6C

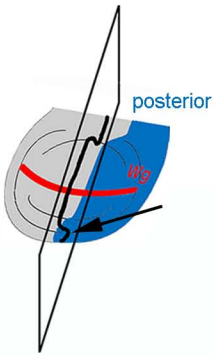

Fig. S4C

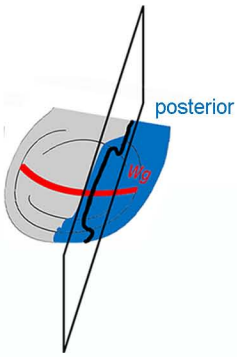

Fig. S4D

Figure S7. Location and orientation of images presented in Figs. 4-6. Schematic representation where images were taken in the wing disc. For Figs. S4C,D, the plane of the section is indicated as it cuts through the disc (black line). In the case of Fig.S4C, the section passes primarily through the anterior compartment (gray), where expression of BiFC constructs is not induced. Only a glancing section through the posterior compartment occurs (blue, arrow), where BiFC is evident in Fig. S4C. In contrast, a parallel adjacent section cuts through posterior tissue (Fig. S4D).

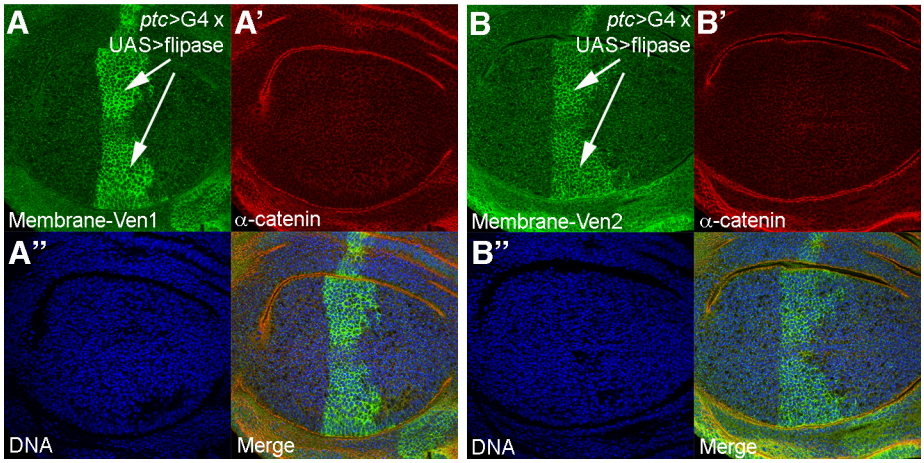

Figure S8. Identification and verification of anti-GFP antiserum recognizing Ven1 and Ven2 fragments. (A,B) *tubulin*-promoter driven expression of membrane-tethered Ven1 or Ven2 fragments was induced by removal of the w+ cassette only in cells expressing *ptc*>Gal4 x UAS>flipase (Materials and Methods). This allows determination of antibody specificity by comparing to cells outside the stripe. Background was enhanced for context.